

Localization of osteoblast inflammatory cytokines MCP-1 and VEGF to the matrix of the trabecula of the femur, a target area for metastatic breast cancer cell colonization

Karen M. Bussard · Noriaki Okita ·
Neil Sharkey · Thomas Neuberger ·
Andrew Webb · Andrea M. Mastro

Received: 12 April 2010 / Accepted: 20 April 2010 / Published online: 6 May 2010
© Springer Science+Business Media B.V. 2010

Abstract Bone likely provides a hospitable environment for cancer cells as suggested by their preferential localization to the skeleton. Previous work has shown that osteoblast-derived cytokines increased in the presence of metastatic breast cancer cells. Thus, we hypothesized that osteoblast-derived cytokines, in particular IL-6, MCP-1, and VEGF, would be localized to the bone metaphyses, an area to which breast cancer cells preferentially traffic. Human metastatic MDA-MB-231 breast cancer cells were inoculated into the left ventricle of the heart of athymic mice. Three to four weeks later, tumor localization within isolated femurs was examined using μ CT and MRI. In addition, IL-6, MCP-1, and VEGF localization were assayed via

immunohistochemistry. We found that MDA-MB-231 cells colonized trabecular bone, the area in which murine MCP-1 and VEGF were visualized in the bone matrix. In contrast, IL-6 was expressed by murine cells throughout the bone marrow. MDA-MB-231 cells produced VEGF, whose expression was not only associated with the breast cancer cells, but also increased with tumor growth. This is the first study to localize MCP-1, VEGF, and IL-6 in bone compartments via immunohistochemistry. These data suggest that metastatic cancer cells may co-opt bone cells into creating a niche facilitating cancer cell colonization.

Keywords Bone · Breast cancer · IL-6 · MCP-1 · Metastasis · VEGF

Karen M. Bussard—Submitted in partial fulfillment of the Ph.D. thesis requirement of The Pennsylvania State University's Graduate Program in Pathobiology.

K. M. Bussard
Department of Veterinary and Biomedical Sciences, The
Pennsylvania State University, University Park, PA 16802, USA

N. Okita · N. Sharkey
Department of Kinesiology, The Pennsylvania State University,
University Park, PA 16802, USA

N. Okita
Department of Mechanical and Nuclear Engineering, The
Pennsylvania State University, University Park, PA 16802, USA

T. Neuberger · A. Webb
Department of Bioengineering, The Pennsylvania State
University, University Park, PA 16802, USA

A. M. Mastro (✉)
Department of Biochemistry and Molecular Biology,
The Pennsylvania State University, 431 S. Frear Building,
University Park, PA 16802, USA
e-mail: a36@psu.edu

Abbreviations

BRMS	Breast cancer metastasis suppressor
CO ₂	Carbon dioxide
DAB	3,3'-Diaminobenzidine
EDTA	Ethylene diamine tetraacetic acid
FBS	Fetal bovine serum
GFP	Green fluorescent protein
hVEGF	Human vascular endothelial growth factor
IL-6	Interleukin 6
IL-8	Interleukin 8
MCP-1	Monocyte chemoattractant protein-1
mIL-6	Murine interleukin 6
mMCP-1	Murine monocyte chemoattractant protein-1
mRNA	Messenger ribonucleic acid
mVEGF	Murine vascular endothelial growth factor
MRI	Magnetic resonance imaging
NIH	National Institutes of Health
PBS	Phosphate buffered saline
PCR	Polymerase chain reaction

TGF- β	Transforming growth factor beta
μ CT	Micro cat scan
VEGF	Vascular endothelial growth factor

Introduction

In the United States, breast cancer accounts for 1 in 3 cancers diagnosed in women [1]. Breast cancer preferentially metastasizes to bone, where the five-year survival rate drops from >90% to <10% [1]. Complications induced by skeletal metastases include bone pain, fractures, and hypercalcemia [2].

Bone provides structural support for the body [3] and consists of cortical or trabecular bone. Cortical bone composes the dense outer layer of bone [3]. Trabecular bone, with a porous matrix, is metabolically active, located near the ends of long bones (e.g. femur), and has the highest rate of bone turnover [3]. Approximately 50% primary and 80% of recurring breast cancer metastasize to the skeleton [4], with cells preferentially trafficking early to the ends of long bones (metaphyses) [5]. Specific chemoattractants to bone metaphyses have yet to be identified; however, known breast cancer maintenance factors, such as TGF- β , are stored in the matrix [6]. Bone cells additionally contain growth factors, cytokines, and chemotactic factors that attract, retain, and support cancer cell proliferation [7, 8].

In the adult, there is a precise balance between osteoblast bone deposition and osteoclast-bone resorption with no net bone gain or loss [9]. However, when metastatic breast cancer cells invade bone, bone remodeling is disrupted and bone loss exceeds deposition [10]. Bisphosphonates are used to block osteoclast-bone resorption, but this treatment is not curative [11]. Lesions are not healed [12]. Current models implicate cytokines and chemokines produced by cancer cells as keys to understanding bone metastatic breast cancer. While cancer cells undoubtedly play an important role in bone metastatic breast cancer, we have evidence that *osteoblasts* are directed by metastatic breast cancer cells to produce cytokines that maintain cancer cells as well as differentiate and activate osteoclasts [13].

We previously reported that osteoblasts exposed to metastatic breast cancer cells showed increased apoptosis and suppression of bone matrix proteins [14, 15]. In addition, the osteoblasts undergo an inflammatory stress response and produce cytokines that can attract osteoclast precursors necessary for osteolysis [13]. We believe these cytokines are an essential part of a unique niche allowing for breast cancer cell colonization of bone. Previously, it was reported that osteoblasts normally produce MCP-1,

IL-6, and VEGF mRNA [16–18], where the levels of these cytokines increase in murine models of osteomyelitis and in infected human bone tissue [19, 20]. The precise location of these cytokines within bone; however, is unknown. Therefore, we sought to determine the presence of IL-6, MCP-1, and VEGF in the microenvironment of the femurs of mice inoculated with human metastatic breast cancer cells that metastasize to the bone. We hypothesized that IL-6, VEGF, and MCP-1 would be found in bone metaphyses compared to the diaphysis.

Materials and methods

Cells

Breast cancer cell variants

To allow detection via fluorescence microscopy, cell lines expressing green fluorescent protein (GFP) were utilized. MDA-MB-231W-GFP cells are a human metastatic breast cancer line derived from a pleural effusion [21]. MDA-MB-231BRMS-GFP cells are a human variant with suppressed metastasis to bone and other organs [22]. Both cell lines were a gift from Dr. Danny Welch, University of Alabama, Birmingham. MDA-MB-231PY-GFP cells are comparable to MDA-MB-231W-GFP cells [21]. MDA-MB-231PY-GFP and MDA-MB-231BO-GFP are the GFP variants of MDA-MB-231PY and MDA-MB-231BO-GFP bone-seeking metastatic breast cancer cells, respectively [23]. Both lines were a gift from Dr. Patricia Steeg, National Cancer Institute at the National Institutes of Health, Bethesda, Maryland, with approval from Dr. Toshiyuki Yoneda, University of Texas Health Science Center, San Antonio, Texas. All cells were maintained in a breast cancer growth medium of DMEM (Mediatech, Manassas, VA), 5% neonatal FBS (Cansera, Roxdale, Ontario), and penicillin 100 U/ml/streptomycin 100 μ g/ml (Sigma, St. Louis, MO) except for MDA-MB-231PY-GFP and MDA-MB-231BO-GFP, which were maintained in 10% neonatal FBS. All cells were maintained in an antibiotic-free environment for at least three passages immediately prior to use, and tested negative for *Mycoplasma* spp. infection (TaKaRa Bio, Inc., Shiga, Japan).

Intracardiac injections

Female athymic mice (Harlan Sprague–Dawley, Indianapolis, IN), aged 6 weeks, six per experimental group, were anesthetized and inoculated with a MDA-MB-231-GFP variant at 3×10^5 cells/200 μ l into the left cardiac ventricle as previously described [5] (Table 1). Three or four weeks post-injection, mice were euthanized via CO₂

Table 1 Murine IL-6, MCP-1, VEGF, and human VEGF cytokine expression in femurs of athymic mice inoculated with MDA-MB-231-GFP human metastatic breast cancer cell variants

Number of mice	Uninoculated	MDA-MB-231W-GFP	MDA-MB-231PY-GFP	MDA-MB-231BO-GFP	MDA-MB-231BRMS-GFP
With fluorescent foci in the bone ^a	0/4	3/5	3/6	3/6	4/5
With mIL-6 in the bone marrow	3/3	3/3	3/3	2/2 ^b	3/3
With mMCP-1 in the femur metaphyses	3/3	3/3	2/3	2/2 ^b	3/3
With mVEGF in the femur metaphyses	3/3	3/3	2/3	2/2 ^b	3/3
With hVEGF in the femur	0/3	1/3	2/3	0/2 ^b	1/3

Shown are the number of mice with conditions as specified versus the total number examined

^a Via fluorescence stereomicroscopy

^b Third mouse designated for immunohistochemistry died prior to experiment end

inhalation. Mice were maintained under the guidelines of the NIH and The Pennsylvania State University. All protocols were approved and monitored by the Institutional Animal Care and Use Committee.

In preparation for the study of bone architecture and magnetic resonance imaging (MRI), whole femurs and tibiae cleaned free of soft tissue were wrapped in phosphate buffered saline (PBS)-soaked gauze and stored at -20°C . For use, bones were thawed and removed from gauze wraps.

Fluorescence stereomicroscopy

Femurs and tibiae were harvested, dissected free of soft tissue, and examined by fluorescence stereomicroscopy using a Nikon SMZ 1500 Fluorescence Stereoscope (Nikon Instruments, Inc., Melville, NY) with a P-HR PLAN APO 1 \times objective and 10 \times eyepiece, allowing for 12–120 \times magnification, and an ENDOW GFP Longpass GFP fluorescence filter ($\lambda_{\text{excitation}} = 488 \text{ nm}$; $\lambda_{\text{emission}} = 515 \text{ nm}$; Chroma Technology Corporation, Rockingham, VT). Photographs were taken using a Nikon CoolPix 8400 digital camera with a 24–85 mm zoom lens (Nikon Instruments, Inc.).

Bone preparation for immunohistochemistry

One femur from each of three mice per MDA-MB-231-GFP variant experimental group was utilized for immunohistochemistry (Table 1). Dissected femurs were fixed for 24–48 h at 4°C in 4% paraformaldehyde (VWR, Bridgeport, NJ), and decalcified for an additional 24–48 h at 4°C with 0.5 mol/l EDTA in dH_2O (Sigma) [5, 24]. For embedding, bones were soaked in 30% sucrose in PBS for 24 h, placed in Shandon CryomatrixTM embedding medium (Thermo Shandon, Waltham, MA), and snap frozen in liquid nitrogen using the Gentle-Jane[®] SnapFreezing technique

(Instrumedics Inc., Hackensack, NJ). Frozen samples were wrapped in aluminum foil, and stored at -20°C .

CryoJane frozen section preparation

Cryosectioning was performed on a Leica CM1900 Cryostat (Leica, Inc., Nussloch, Germany) equipped with the CryoJane Frozen Sectioning Kit (Instrumedics Inc.). For sectioning, femurs were oriented with the end proximal to the hip pointed toward the blade. Ten micron thick longitudinal sections were cut using a Diamond High Profile Knife (C.L. Sturkey, Lebanon, PA). Pre-chilled adhesive transfer tape windows (Instrumedics Inc.) were used to transfer cut sections onto pre-chilled adhesive coated slides (CJ4X adhesive coated slides; Instrumedics Inc.). Three to four bone sections were placed onto each slide. Bone sections were permanently bonded to slides with three flashes of ultraviolet light. Transfer tape windows were removed, and slides stored in slide boxes at -20°C . In some cases, poly-L-lysine coated slides were also utilized.

Immunohistochemistry

Bone sections of femurs from mice euthanized 3 or 4 weeks post cancer cell inoculation were allowed to equilibrate to room temperature for at least 30 min prior to use. Sections were circled with an ImmEdge Hydrophobic Barrier Pen (Vector Laboratories, Burlingame, CA), and permeabilized for 10 min using 0.2% Triton-X (Sigma) in PBS. Sections were treated with hyaluronidase (1 mg/ml in TBS; Sigma) for 30 min at 37°C for antigen retrieval. Endogenous peroxidase activity was blocked with PEROXIDAZED (Biocare Medical, Concord, CA) for 10 min at room temperature. Non-specific binding was blocked with 10% donkey serum in TBS-X (Sigma) for 1 h. Slides were incubated for 1 h with either primary rabbit polyclonal anti-GFP IgG (1:1500; Molecular Probes, Eugene,

OR), rabbit polyclonal anti-mouse MCP-1 (30 µg/ml; Abcam, Cambridge, MA), rabbit polyclonal anti-mouse CD41 (1:100; Abcam), goat polyclonal anti-mouse VEGF (25 µg/ml; R&D Systems, Minneapolis, MN), goat polyclonal anti-human VEGF (10 µg/ml; R&D Systems), or goat polyclonal anti-mouse IL-6 (30 µg/ml; R&D Systems). A secondary antibody of either biotinylated donkey anti-rabbit (1:750; Abcam) or biotinylated donkey anti-goat (1:2500; Abcam) was applied for 1 h. Sections were incubated with avidin-horseradish peroxidase for 20 min (Covance, Dedham, MA), and visualized using either a Biogenex liquid 3,3'-diaminobenzidine (DAB) kit (Biogenex, San Ramon, CA) or a liquid DAB kit (Sigma). Sections were counterstained using Gill's Hematoxylin (Vector Laboratories) and mounted with VectaMount (Vector Laboratories). Sections without the primary antibody and non-cancer-bearing murine bones served as negative controls. Images were viewed using a Leitz Dialux 20 light microscope (Leitz, Wetzlar, Germany), which includes a 10× eyepiece, with either a 6.3× NPI Leitz (Leitz) or 25× Ph2 Plan Carl Zeiss (Carl Zeiss MicroImaging, Inc., Thronwood, NY) objective allowing for 63–250× magnification. A Leitz GFP fluorescence filter was fitted to the microscope ($\lambda_{\text{excitation}} = 488 \text{ nm}$; $\lambda_{\text{emission}} = 515 \text{ nm}$, Leitz). The Leitz Dialux 20 microscope was fitted to mount a Nikon CoolPix 8400 digital camera with a 24–85 mm zoom lens (Nikon Instruments, Inc.).

Bone architecture/MRI

For bone architecture studies, thawed bones from mice 4 weeks post cancer cell inoculation were arranged in a 30 mm sample holder of a µCT40 Desktop MicroCT (µCT) Scanner (SCANCO Medical AG, Zürich, Switzerland) and scanned their entire length. Slices were acquired using machine settings of 55 kVp, 145 µA and 200 ms integration times. Images were reconstructed in 2048 × 2048 pixel matrices and stored in 3D arrays with an isotropic voxel size of 15.4 µm. A threshold value equivalent to 25% of the maximal gray scale was chosen to identify bone tissue from background. Company-provided software and custom scripts were utilized to view images, create three-dimensional models of the bones and determine trabecular bone volumes in the metaphyseal regions harboring tumors.

For MRI analyses, whole femurs from mice 4 weeks post cancer cell inoculation were removed from decalcification solution and immersed in a PBS solution containing 1% v/v gadoteridol (279.3 mg/ml) contrast agent (ProHance[®], Bracco Diagnostics, Inc., Princeton, NJ) for at least 3 days. Images were acquired on a 14.1 T vertical bore MRI system (Varian Inc, Palo Alto, CA). The T_1 and T_2 relaxation times

of PBS with contrast agent were determined with standard inversion recovery and spin echo methods, giving values of 250 and 17 ms, respectively. The short T_1 enabled a short repetition time of 200 ms to be used for the three-dimensional spin echo imaging sequence. Using a field of view of 16×5×5 mm³ and matrix size of 512×142×142, a resolution of 29×35×35 µm³ was obtained. The total scan time was 13.5 h with 12 signal averages. By choosing an echo time of 19.3 ms, the T_2 contrast was high enough to clearly delineate clearly cancerous regions from healthy tissue. After zero filling the raw data by a factor of two and reconstructing the images in MATLAB (The Mathworks, Bolder, CO, USA) via an inverse three-dimensional Fourier transform, the dataset was imported into AMIRA (Mercury Computer Systems Inc., Chelmsford, MA, USA) and segmentation of the bone and infiltrated area performed based on intensity levels. Finally, the ratio of total bone volume to cancerous volume was calculated based on the segmentation.

Results

Metastatic lesions were present in mice inoculated with MDA-MB-231-GFP breast cancer variants

Four approaches were used to localize tumor cells within bone: µCT, MRI, fluorescence, and immunohistochemistry. At least 50% of mice inoculated with MDA-MB-231-GFP cell variants showed foci in the femurs as detected by fluorescence stereomicroscopy (Table 1; MDA-231W: 3/5 mice; MDA-231PY: 3/6 mice; MDA-231BO: 3/6 mice; MDA-231BRMS1: 4/5 mice.). Uninoculated mice remained cancer-free (Table 1). Three femurs per experimental group were chosen at random (fluorescent foci were not visible in all) to utilize for immunohistochemistry. Murine IL-6 (mIL-6), murine MCP-1 (mMCP-1) and murine VEGF (mVEGF) were typically found in the femurs of non-cancer-bearing and cancer-bearing mice (Table 1). All uninoculated, and MDA-231W-GFP, MDA-231BO-GFP, and MDA-231BRMS-GFP inoculated mice expressed mMCP-1 and mVEGF, whereas two out of three of MDA-231PY-GFP inoculated mice expressed mMCP-1 and mVEGF. Human VEGF (hVEGF) expression was only found in mice inoculated with cancer cells and expression correlated with tumor size (Table 1).

Metastatic breast cancer cells localized to the trabecular bone

Tibia from uninoculated and cancer-bearing mice 3 weeks post-inoculation were photographed and scanned using a µCT40 Desktop Cone-Beam MicroCT Scanner. Three-

dimensional models of the bone, trabeculae, and tumor, if present, were constructed and quantitated. Tumors in cancer-bearing tibia were found in bone metaphyses in contrast to the diaphysis. A tumor in the bone metaphysis, as indicated by arrows and GFP, is illustrated in a representative tibia (posterior view, Fig. 1a, b). The tumor was localized to the trabecular bone (Fig. 1c, d, arrow; compare to control Fig. 1e, f). Interestingly, trabecular bone volume as calculated in the cancer-bearing tibia, was 75% less (Fig. 1c, inset) than a tibia from an uninoculated mouse (Fig. 1e, inset). Results were similar among assayed tibiae from mice inoculated with MDA-MB-231-GFP variants.

Tumor volume was estimated from MRI

MRI was used to confirm tumor location and determine tumor volume. Femurs were photographed using light microscopy (Fig. 1g, k) and fluorescence stereomicroscopy (Fig. 1h, l). Tumors were highly heterogeneous in structure. As an example, a tumor was detected in the distal metaphysis of an MDA-MB-231W-GFP cancer-bearing mouse 4 weeks post-inoculation. The signal from the tumor, shown as a white mass in distal metaphysis (Fig. 1m), was segmented (Fig. 1n). Tumor to bone volume was estimated to be 2.7%, with the absolute volume of the tumor estimated to be

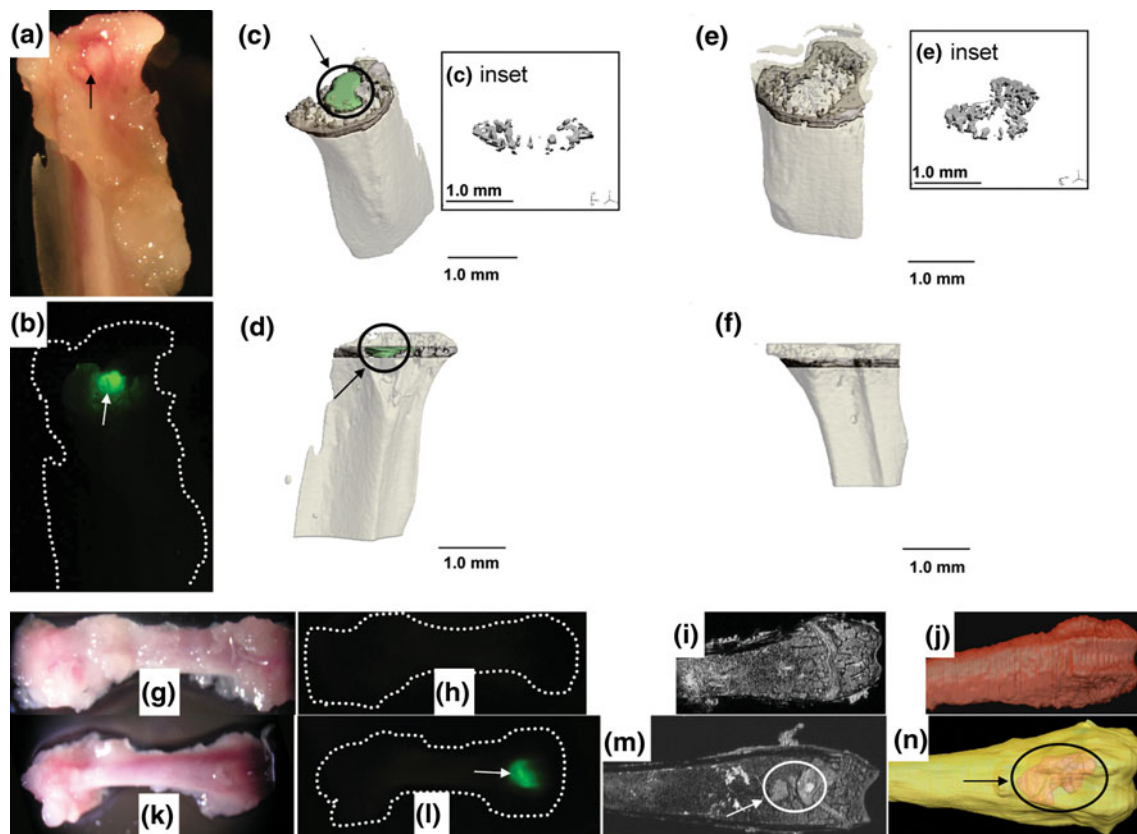


Fig. 1 Human metastatic breast cancer cells colonize the trabecular bone. Six-week-old female athymic mice (6 per group) were inoculated in the left cardiac ventricle with MDA-MB-231-GFP metastatic breast cancer cell variants. Control mice were left uninoculated. Three weeks post-inoculation, mice were euthanized, femurs and tibiae harvested, cleaned free of soft tissue, photographed using a fluorescent stereomicroscope, and stored as described in the materials and methods. A μ CT40 Desktop MicroCT Scanner was used to assess bone architecture. **a** The light microscopy image of a cancer-bearing tibia, where **b** a tumor was detected in the metaphyseal region proximal to the knee by fluorescence stereomicroscopy. **c, d** a three-dimensional μ CT reconstruction of the metaphyseal region illustrates that the tumor (arrow) localized in the trabecular bone (dark grey) in an anterior view (c) and posterior view (d). **c (inset)** The volume of trabecular bone in the cancer-bearing tibia was reduced compared to control (**e, inset**). Tibia from an uninoculated mouse with trabecular bone (grey) as seen from an **e** anterior and **f** posterior view. Scans

were performed independently on one non-cancer-bearing tibia and femur and one cancer-bearing tibia and femur from mice inoculated with each MDA-MB-231-GFP cancer cell variant. Tibiae and femurs were from different mice. Femurs were imaged via MRI to assess for tumor cell presence and volumetric analyses. **g, k** Light microscopy image and **h, l** corresponding fluorescent microscopy image of representative control (**g–j**) and MDA-MB-231W-GFP cancer-bearing (**k–n**) murine femurs. In the cancer-bearing femur, tumor cells were localized in the area distal to the hip (**l, arrow**). **i, m** Corresponding MRI images. In the cancer-bearing femur, the tumor is seen as a large white object in the distal metaphysis (**m, arrow**). **J, N** Corresponding three-dimensional image reconstructions. Femur from an uninoculated mouse (**j**) is cancer-free, whereas the tumor is illustrated in situ in the cancer-bearing femur (**n**). Three control and three MDA-MB-231W-GFP cancer-bearing femurs were scanned. Shown are representative experiments

1.32 mm³. Tumor localization within the bone was similar among assayed femurs from mice bearing the different cancer cell variants. Femurs from uninoculated mice showed no tumors (e.g. Fig. 1g–j).

Murine MCP-1 and VEGF were localized in the trabecular bone in both control and cancer-bearing mice

Immunohistochemistry was used to detect the presence of mVEGF and mMCP-1 in the femur. A xenograft system (human cancer cells inoculated into mice) permitted species-specific cytokine detection. Both mVEGF and mMCP-1 were found in the trabecular bone matrix within the proximal

(Fig. 2a, b) and distal (Fig. 2c, d) femoral metaphyses. mMCP-1 and mVEGF were detected in 100% of uninoculated, MDA-231W-GFP, MDA-231BO-GFP, and MDA-231BRMS-GFP inoculated mice examined. In one femur of the three MDA-231PY-GFP inoculated mice examined, mMCP-1 and mVEGF were not detected for unknown reasons (Table 1). Furthermore, neither mMCP-1 or mVEGF were found associated with cells in the bone marrow.

Murine MCP-1 and VEGF were localized in the matrix near the trabecular bone, but not in the bone shaft

Both mMCP-1 and mVEGF were found in a 10–50 µm wide strip in cortical bone of the metaphyseal periphery

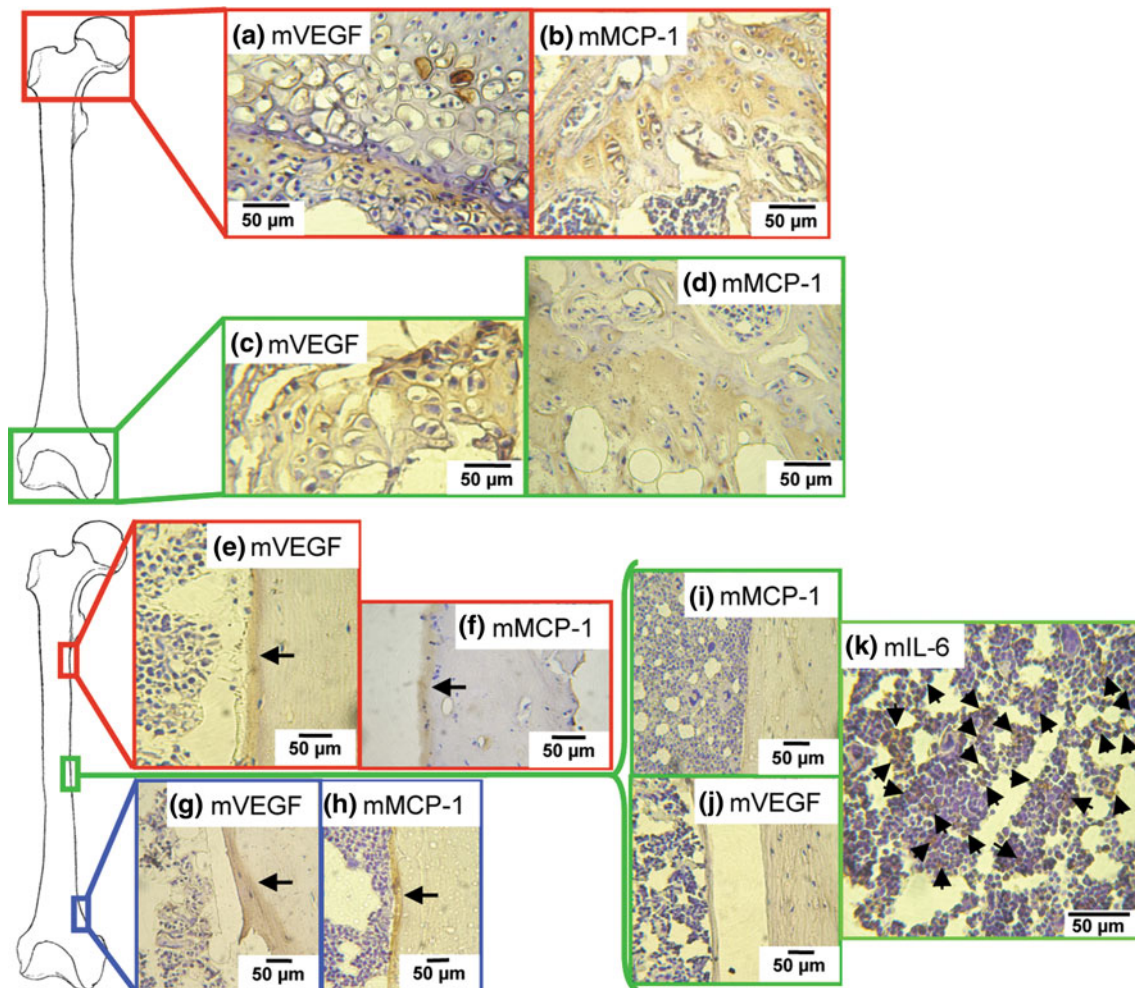


Fig. 2 Murine MCP-1, IL-6, and VEGF were localized in the bone microenvironment. Femurs harvested from athymic nude mice, inoculated as described in the “Materials and methods” section, were cryosectioned in 10 µm thick longitudinal sections, and stained for murine VEGF, murine MCP-1, or murine IL-6 via immunohistochemistry, and visualized using a brown DAB chromogen stain. Slides were counterstained using Gill’s Hematoxylin. **a, c** Murine VEGF and **b, d** murine MCP-1 were localized in trabecular bone of the proximal and distal femur. **e, g** Murine VEGF and **f, h** murine

MCP-1 were localized in cortical bone of the proximal and distal metaphyses. Neither **i** murine MCP-1 nor **j** murine VEGF were localized in cortical bone of the diaphysis. **k** Murine IL-6 was localized throughout the bone marrow. Murine IL-6 was not present in the trabecular bone or the cortical bone matrix. At least three independent sections were stained per bone, and three bones examined per uninoculated or inoculated MDA-MB-231-GFP variant. Shown are representative sections

(Fig. 2e–h). These cytokines were seen in both the proximal (mVEGF, Fig. 2e; mMCP-1, Fig. 2f) and distal (mVEGF, Fig. 2g; mMCP-1, Fig. 2h) regions of murine femurs. Neither mMCP-1 or mVEGF were detected in the diaphysis (mMCP-1, Fig. 2i; mVEGF, Fig. 2j). mMCP-1 and mVEGF expression appeared to be similar between non-cancer-bearing and cancer-bearing femur sections of the MDA-MB-231-GFP breast cancer cell variants (Table 1). Furthermore, localization was not different among the mice inoculated with different variants of MDA-MB-231 cells.

Murine IL-6 was localized in the bone marrow

Femur sections were also stained for mIL-6 via immunohistochemistry. Interestingly, mIL-6 was not present in the

matrix or localized to the metaphyseal regions of the femur. Instead, mIL-6 was found in cells throughout the bone marrow (Fig. 2k), which appeared to be hematopoietic cells. This distribution was seen in all femurs examined (Table 1).

Murine cytokine expression was not detected immediately adjacent to cancer colonies

We examined areas of the bone adjacent to the metastases as well as areas further away for the presence of mMCP-1, mVEGF, and hVEGF cytokines. In the example shown (Fig. 3), MDA-MB-231W-GFP cells were detected both by fluorescence stereomicroscopy (Fig. 3a) and immunohistochemistry after staining with anti-GFP (Fig. 3b) in

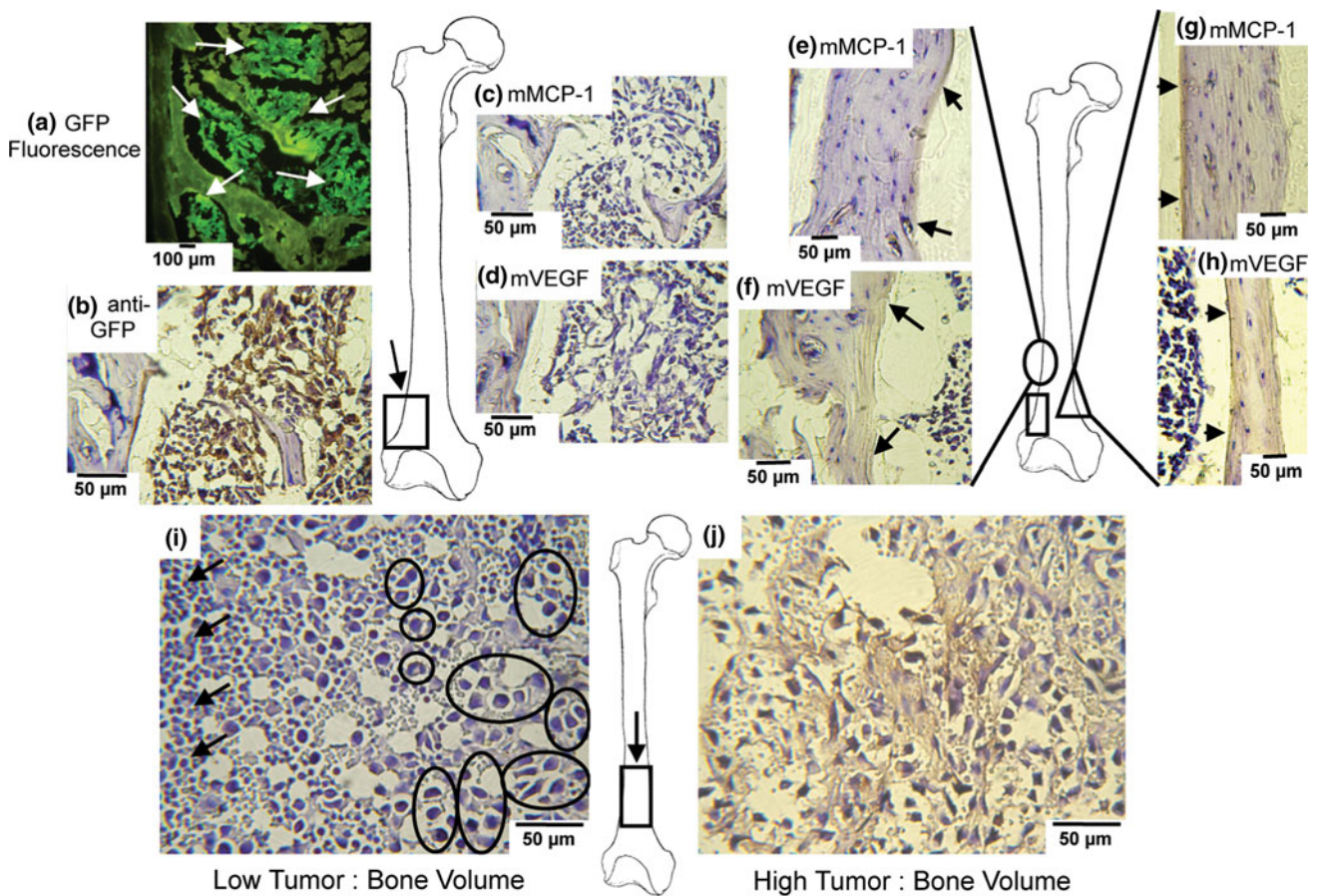


Fig. 3 Cytokine expression was altered with tumor cell presence. Femur sections from athymic mice were prepared as described in “Materials and methods” section. Sections were photographed and stained via immunohistochemistry for murine MCP-1, murine VEGF, human VEGF, or anti-GFP IgG. **a** The fluorescent microscope image of tumor cells present in the trabecular bone of the distal femoral metaphysis. **b** Corresponding anti-GFP IgG image. Neither **c** murine MCP-1 or **d** murine VEGF were detected within ~150 μm of the tumor. **e** Murine MCP-1 and **f** murine VEGF were detected in the cortical bone proximal to the tumor (*circle*) and present in a gradient extending away from the tumor. **g** Murine MCP-1 and **h** murine

VEGF were detected in the cortical bone (*triangle*) of the side opposite the tumor. In this example, the tumor was located in the trabecular bone of the distal metaphysis (*rectangle, arrow*). **i** Human VEGF expression was not detected in the femur from a mouse 3 weeks post-inoculation. Large human tumor cells (*right, circles*) were present with small murine bone marrow cells (*left, arrows*). **j** Human VEGF expression increased with tumor volume in the femur from a mouse 4 weeks post-inoculation. At least three independent sections were stained per bone, and three bones examined per uninoculated or inoculated MDA-MB-231-GFP. Shown are representative sections

trabecular bone of the distal metaphysis. In this femur, tumor cells were seen adjacent to cortical bone and slightly superior to trabecular bone (Fig. 3a, b). Tumor cells were also seen in the marrow cavity apart from cortical bone (Fig. 3b). When mMCP-1 (Fig. 3c) and mVEGF (Fig. 3d) presence was assayed via immunohistochemistry in cancer-bearing sections, they were not found immediately adjacent to the tumors, i.e. within $\sim 150 \mu\text{m}$ of the tumor mass. However, they were detected in areas slightly beyond the tumor mass. In a representative femur (Fig. 3e–h), a tumor was detected in the distal metaphysis (rectangle). In the region immediately proximal to the tumor cells (circle), both mVEGF and mMCP-1 were detected in cortical bone. Interestingly, both cytokines were expressed in a gradient, i.e. regions immediately superior to the tumor expressed more cytokine than within the tumor (mMCP-1, Fig. 3e mVEGF, Fig. 3f). Furthermore, the cytokine gradient was specific to the area immediately adjacent to the tumor. When cortical bone on the opposite side of the femur was examined, both mMCP-1 (Fig. 3g) and mVEGF (Fig. 3h) were present in defined strips. The lack of murine cytokines immediately adjacent to the tumor metastases may reflect an increase in the loss of osteoblasts in the area by 4 weeks as previously reported [5]. This cytokine-clear area was observed in femurs of mice independently inoculated with each of the cancer cell variants.

Human VEGF expression increased with tumor presence

In contrast to mVEGF, which was located in the bone matrix (Fig. 2a, c, e, g), hVEGF expression was associated with the tumor cells (Fig. 3i, j). As the tumor colony increased, hVEGF expression was concurrently amplified (Fig. 3j). Increased hVEGF expression was observed in mice inoculated with MDA-MB-231W-GFP and MDA-MB-231PY-GFP metastatic or MDA-MB-231BRMS-GFP non-metastatic breast cancer cells. Under study conditions, increases in tumor-derived VEGF were not seen in femurs from MDA-MB-231BO-GFP or MDA-MB-231BRMS-GFP inoculated mice (Table 1). MDA-MB-231BO-GFP, in spite of being bone seeking, were found to not grow well under assay conditions.

Discussion

Despite the prevalence of bone metastatic breast cancer, little is known as to why bone is a preferred site of metastasis [25]. It is suggested that bone is an attractive site for cancer metastasis due to its highly vascularized, metabolically active environment. Bone-depositing osteoblasts and bone-resorbing osteoclasts contribute to bone

remodeling through a variety of cytokines, chemokines, and growth factors. These same molecules appear to be important for tumor cell metastases. Cancer cell-secreted IL-8 and IL-6 have been implicated with bone metastasis and stimulation of osteoclast differentiation, leading to increased bone resorption and release of cancer cell survival factors from bone [26, 27]. Furthermore, Kinder et al. [13] demonstrated metastatic breast cancer cells co-opt osteoblasts into increasing more IL-6 and MCP-1, which are reported to be involved in breast cancer cell migration, survival, and osteoclast activation [28, 29]. Similarly, VEGF has been shown to increase breast cancer survival, and is an indicator of poor prognosis for patients with breast disease [30, 31]. For the study discussed here, the localization of murine IL-6, murine MCP-1, murine VEGF, and human VEGF in the bone microenvironment was assessed via immunohistochemistry.

A pleiotropic cytokine involved in bone remodeling, IL-6 has been implicated in osteoclastogenesis [16] as well as Paget's disease [32]. IL-6 increases T47D breast cancer cell migration in vitro [33], and enhances epithelial tumor cell survival [34]. Unlike MCP-1 and VEGF, murine IL-6 is not active on human cells. In the xenograft model used in this study, IL-6 is likely directed toward murine osteoclasts and osteoclast progenitors, the cells responsible for bone degradation. In a syngeneic system, IL-6 can act both on cancer cells and on osteoclasts [35]. MCP-1, a monomeric polypeptide member of the CC chemokine superfamily, is normally produced by osteoblasts [36], attracts inflammatory molecules such as tumor associated macrophages [35], and increases cancer cell migration and survival [37]. A dimeric protein related to the PDGF family of growth factors, VEGF increases blood vessel cell permeability, is produced by monocytes [35], macrophages [35], osteoblasts [38], and osteoclasts [38], prevents apoptosis in endothelial cells of newly formed vessels [39], and promotes epithelial tumor cell survival [40].

An exhaustive survey of the literature suggests that this is the first study to localize mMCP-1, mVEGF, and hVEGF to the bone metaphysis and mIL-6 to the bone marrow of murine femurs by immunohistochemistry. Specifically, we show that mMCP-1 and mVEGF were present in the matrix of the trabeculae of bone metaphyses, an area to which breast cancer cells preferentially traffic [5], and not in the cortical bone shaft. Furthermore, utilizing μCT , we showed that metastatic breast cancer cells localized within trabecular bone of the metaphyseal region. Interestingly, no differences in the areas of cytokine *localization* via immunohistochemistry were observed between non-cancer-bearing and cancer-bearing mice except that in the area immediately adjacent to the tumor, cytokine expression was depressed. This observation may be explained by the loss of osteoblasts late in the metastatic process [5].

Furthermore, there were no apparent differences in the amount of cytokines present in femurs from control or mice inoculated with any of the cancer variants. The apparent lack of quantitative differences may be due to the loss of secreted, soluble cytokines during the processing of the bones. As was noted, both mVEGF and mMCP-1 were present in the bone matrix whereas tumor-derived hVEGF was found associated with the tumor cells in the bone marrow cavity. These data as a whole support the idea that bone metastatic breast cancer cells colonize regions of high bone turnover that express MCP-1 and VEGF. In fact, the increase in human cytokines may be caused by a decrease in bone content due to increased osteoblast apoptosis as reported by Mastro et al. [14]. These cytokines may aid in tumor cell colonization and survival at secondary sites. Furthermore, endogenous VEGF, MCP-1, as well as IL-6, may aid in ‘priming’ the metaphyseal bone microenvironment for cancer cell arrival. This idea has been postulated in recent literature as the formation of a ‘pre-metastatic niche’ [39, 41].

As reviewed by Kaplan et al. [41], and Wels et al. [39], the possibility that tumor cells are capable of priming distant sites has been debated for over a century, when Stephen Paget first described the ‘seed and soil’ hypothesis. Paget stated “When a plant goes to seed, its seeds are carried in all directions; but they can only grow if they fall on congenial soil [42].” Clearly, the microenvironment of secondary locations are crucial in determining whether cancer cells will metastasize to that site, and if cancer cell proliferation is supported. If cancer cells can prime a distant, secondary site for colonization, bone, rich in growth factors, cell adhesion molecules, cytokines, and chemokines, is an optimal location for cancer cell settlement.

In the course of these studies, we have also observed a sharp increase in the number of megakaryocytes in the femurs of cancer-bearing mice [43]. It is possible that megakaryocytes prime the metaphyseal bone for cancer cell arrival and colonization or, conversely, that megakaryocytosis increases in the presence of inflammatory cytokines such as IL-6. This observation is currently being further pursued.

While many unanswered questions remain, the probability of a pre-metastatic niche and/or metastatic signature is likely. Both bone- and tumor-derived MCP-1, VEGF, and IL-6, as examined in this study, have a variety of known targets including osteoclast precursors, osteoclasts, endothelial cells, cancer cells, and osteoblasts [35, 44, 45]. Each of these cells contribute to making the metaphyseal region of bone attractive for metastatic breast cancer cell colonization. Given evidence of the impact of MCP-1, VEGF, and IL-6 on the bone microenvironment, there is little doubt that they are key mediators in bone metastatic breast cancer.

Acknowledgments This work was supported by the U.S. Army Medical and Material Research Command Breast Cancer Program (DAMD 17-02-1-0358 and W81XWH-06-1-0432 to AMM, W81XWH-06-1-0363 to KMB); National Foundation for Cancer Research, Center for Metastasis Research; and The Susan G. Komen Breast Cancer Foundation, BCTR0601044, BCTR104406. The authors would like to thank Jianwen Wei and Donna Sosnoski for their assistance.

References

1. Society AC (2007) Cancer Statistics, 2007. American Cancer Society, Atlanta
2. Guise TA, Kozlow WM, Heras-Herzig A, Padalecki SS, Yin JJ, Chirgwin JM (2005) Molecular mechanisms of breast cancer metastases to bone. *Clin Breast Cancer* 5(Suppl):S46–S53
3. Marks SC, Odgren PR (2002) Structure and development of the skeleton. In: Bilezikian JP, Raisz LG, Rodan GA (eds) *Principles of bone biology*. Academic Press, New York, pp 3–15
4. Solomayer EF, Diel IJ, Meyberg GC et al (2000) Metastatic breast cancer: clinical course, prognosis and therapy related to the first site of metastasis. *Breast Cancer Res Treat* 59(3):271–278
5. Phadke PA, Mercer RR, Harms JF et al (2006) Kinetics of metastatic breast cancer cell trafficking in bone. *Clin Cancer Res* 12:1431–1440
6. Guise TA (2000) Molecular mechanisms of osteolytic bone metastases. *Cancer* 88:2892–2898
7. Canalis E (2003) Osteogenic growth factors. In: Flavin MJ (ed) *Primer on the metabolic bone diseases and disorders of mineral metabolism*, 5th edition. American Society for Bone and Mineral Research, Washington, DC, pp 28–31
8. Kozlow W, Guise TA (2005) Breast cancer metastasis to bone: mechanisms of osteolysis and implications for therapy. *J Mammary Gland Biol Neoplasia* 10(2):169–180
9. Mundy GR, Chen D, Oyajobi BO (2003) Bone remodeling. In: Flavin MJ (ed) *Primer on the metabolic bone diseases and disorders of mineral metabolism*. American Society for Bone and Mineral Research, Washington, DC, pp 46–57
10. Mundy GR (2002) Metastasis to bone: causes, consequences and therapeutic opportunities. *Nat Rev Cancer* 2:584–593
11. Hiraga T, Williams PJ, Mundy GR (2001) The bisphosphonate ibandronate promotes apoptosis in MDA-MB-231 human breast cancer cells in bone metastases. *Cancer Res* 61:4418–4424
12. Taube T, Elomaa I, Blomqvist C et al (1994) Histomorphometric evidence for osteoclast-mediated bone resorption in metastatic breast cancer. *Bone* 15:161–166
13. Kinder M, Chislock EM, Bussard KM et al (2008) Metastatic breast cancer induces an osteoblast inflammatory response. *Exp Cell Res* 314:173–183
14. Mastro AM, Gay CV, Welch DR et al (2004) Breast cancer cells induce osteoblast apoptosis: a possible contributor to bone degradation. *J Cell Biochem* 91:265–276
15. Mercer R, Miyasaka C, Mastro AM (2004) Metastatic breast cancer cells suppress osteoblast adhesion and differentiation. *Clin Exp Metastasis* 21:427–435
16. Black K, Garrett IR, Mundy GR (1991) Chinese hamster ovarian cells transfected with the murine interleukin-6 gene cause hypercalcemia as well as cachexia, leukocytosis and thrombocytosis in tumor-bearing nude mice. *Endocrinology* 128:2657–2659
17. Horowitz MC, Lorenzo JA (2002) *Principles of bone biology*. Academic Press, San Diego
18. Ferrara N, Carver-Moore K, Chen H et al (1996) Heterozygous embryonic lethality induced by targeted inactivation of the VEGF gene. *Nature* 380:439–442

19. Marriott I, Gray DL, Tranguch SL et al (2004) Osteoblasts express the inflammatory cytokine interleukin-6 in a murine model of *Staphylococcus aureus* osteomyelitis and infected human bone tissue. *Am J Pathol* 164:1399–1406
20. Marriott I, Gray DL, Rati D et al (2003) Osteoblasts produce monocyte chemoattractant protein-1 in a murine model of osteomyelitis and infected human bone tissue. *Bone* 37:504–512
21. Cailleau R, Olive M, Cruciger QV (1978) Long-term human breast carcinoma cell lines of metastatic origin: preliminary characterization. *In Vitro* 14:911–915
22. Phadke PA, Vaidya KS, Nash KT et al (2008) BRMS1 suppresses breast cancer experimental metastasis to multiple organs by inhibiting several steps of the metastatic process. *Am J Pathol* 172:809–817
23. Yoneda T, Williams PJ, Hiraga T et al (2001) A bone-seeking clone exhibits different biological properties from the MDA-MD-231 parental human breast cancer cells and a brain-seeking clone in vivo and in vitro. *J Bone Miner Res* 16:1486–1495
24. Harms JF, Budgeon LR, Christensen ND et al (2002) Maintaining GFP tissue fluorescence through bone decalcification and long-term storage. *BioTechniques* 33:1197–1200
25. Bussard KM, Gay CV, Mastro AM (2008) The bone microenvironment in metastasis; what is special about bone? *Cancer Metastasis Rev* 27:41–55
26. Bendre M, Montague DC, Peery T et al (2003) Interleukin-8 stimulation of osteoclastogenesis and bone resorption is a mechanism for the increased osteolysis of metastatic bone disease. *Bone* 33:28–37
27. Guise TA, Chirgwin JM (2003) Transforming growth factor-beta in osteolytic breast cancer bone metastases. *Clin Orthop Relat Res* 415S:532–538
28. Badache A, Hynes NE (2001) Interleukin 6 inhibits proliferation and, in cooperation with epidermal growth factor receptor autocrine loop, increases migration of T47D breast cancer cells. *Cancer Res* 61:383–391
29. Goede V, Brogelli L, Ziche M et al (1999) Induction of inflammatory angiogenesis by monocyte chemoattractant protein-1. *Int J Cancer* 82:765–770
30. Adams J, Carder PJ, Downey S et al (2000) Vascular endothelial growth factor (VEGF) in breast cancer: comparison of plasma, serum, and tissue VEGF and microvessel density and effects of tamoxifen. *Cancer Res* 60:2898–2905
31. Liang Y, Brekken RA, Hyder SM (2006) Vascular endothelial growth factor induces proliferation of breast cancer cells and inhibits the anti-proliferative activity of anti-hormones. *Endocr Relat Cancer* 13:905–919
32. Roodman GD, Kurihara N, Ohsaki Y et al (1992) Interleukin 6. A potential autocrine/paracrine factor in Paget's disease of bone. *J Clin Invest* 89:46–52
33. Badache A, Hynes NE (2001) Interleukin 6 inhibits proliferation and, in cooperation with an epidermal growth factor receptor autocrine loop, increases migration of T47D breast cancer cells. *Cancer Res* 61(1):383–391
34. Kishimoto T (2005) Interleukin-6: from basic science to medicine—40 years in immunology. *Annu Rev Immunol* 23:1–21
35. Fitzgerald KA, O'Neill LAJ, Gearing AJH et al (2001) The cytokine facts book. Academic Press, San Diego
36. Graves DT, Jiang Y, Valente AJ (1999) The expression of monocyte chemoattractant protein-1 and other chemokines by osteoblasts. *Front Biosci* 4:D571–D580
37. Ueno T, Toi M, Saji J et al (2000) Significance of macrophage chemoattractant protein-1 in macrophage recruitment, angiogenesis, and survival in human breast cancer. *Clin Cancer Res* 6:3282–3289
38. Tombran-Tink J, Barnstable CJ (2004) Osteoblasts and osteoclasts express PEDF, VEGF-A isoforms, and VEGF receptors: possible mediators of angiogenesis and matrix remodeling in the bone. *Biochem Biophys Res Commun* 316:573–579
39. Wels J, Kaplan RN, Rafii S et al (2008) Migratory neighbors and distant invaders: tumor-associated niche cells. *Genes Dev* 22:559–574
40. Wang D, Wang H, Guo Y et al (2006) Crosstalk between peroxisome proliferator-activated receptor gamma and VEGF stimulates cancer progression. *Proc Natl Acad Sci USA* 103:19069–19074
41. Kaplan RN, Psaila B, Lyden D (2006) Bone marrow cells in the 'pre-metastatic niche': within bone and beyond. *Cancer Metastasis Rev* 25:521–529
42. Paget S (1889) The distribution of secondary growths in cancer of the breast. *Cancer Metastasis Rev* 8:98–101
43. Bussard KM (2008) Unpublished observations
44. Kurihara N, Bertolini D, Suda T et al (1990) IL-6 stimulates osteoclast-like multinucleated cell formation in long term human marrow cultures by inducing IL-1 release. *J Immunol* 144:4226–4230
45. Gabrilovich DI, Dikov MM (2003) Vascular endothelial growth factor. In: Thomson AW, Lotze MT (eds) *The cytokine handbook*, 4th edn. Academic Press, Amsterdam, pp 1017–1034